Photophysics of Sulfur-Containing Centers on AgBr Surfaces

Alfred P. Marchetti,* Ken Lushington, and Roger Baetzold

Imaging Materials and Media, R&D, Eastman Kodak Company, Rochester, New York 14650-1735

Received: May 15, 2002; In Final Form: October 18, 2002

Silver halide microcrystals, the basic element in photographic products, are commonly reacted with labile sulfur-containing compounds to increase their photographic efficiency (speed). Such "sulfur-sensitized" AgBr microcrystals have been examined with computational and photophysical techniques. Density functional and lattice-relaxation computations have given estimates of the optical transition energies and the electron- and hole-trapping abilities of a number of small sulfur-containing clusters that may be deposited on, or buried in, an AgBr surface. These data indicate that single sulfides, whatever their structure, are not deep traps for electrons or holes. Disulfides, in general, can trap holes and certain structures; for example, a disulfide at a double-kink site can trap electrons. Computations indicate that single sulfides substituted for a halogen in the (001) surface and charge compensated with an interstitial silver ion in the surface or in the bulk do not trap electrons; neither do disulfides in the bulk. A single sulfide substituted for a bromide at a positive kink and compensated with an interstitial silver ion appears to be capable of initiating the formation of small, stable silver clusters (Ag_n, $n \approx 4$) that become "latent image", the centers that eventually lead to a visible photographic image. Photographic data from sulfur-sensitized AgBr microcrystals indicate that the optimum formal sulfur level is about 10 000 S atoms/μm^2. Radio-frequency photoconductivity measurements show that deposited sulfur centers trap photoelectrons. The optimum and higher levels of sulfur deposited on the surface of AgBr microcrystals produce an absorption band (∼525 nm) and associated low-temperature luminescence (∼725 nm). The luminescence lifetime behavior and ODMR data clearly indicate that this sulfur-related absorption and emission is due to a donor−acceptor processes. ODMR spectra obtained by monitoring the intrinsic AgBr luminescence (590 nm) have a resonance that is assigned to a Ag_2^+ center. This Ag_2^+ species is thought to arise from a silver dimer associated with a sulfur species at the surface.

Introduction

The process of reacting labile sulfur and/or gold compounds with silver halide microcrystals to increase photographic efficiency (speed) is known as chemical sensitization. Sensitization with sulfur alone increases the efficiency (speed) of the photographic system by as much as 10-fold, and sulfur sensitization is applied in a large majority of photographic products. The structure and photophysical functions of most of the species thus produced are not known! A great deal of experimental work, some of which will be reviewed below, has been carried out in an attempt to elucidate the structure and the behavior of these centers. However, to date no semiquantitative understanding of chemical sensitization exists.

In the last several years, progress has been made on defining the structure and function of the relatively simple centers that are created upon reduction sensitization, which forms small silver clusters on AgBr surfaces.[1] A combination of photophysical techniques and computational methods yielded a self-consistent and tested picture of several of the centers created upon reduction sensitization. For example, it was shown that the functioning of an Ag_2 center depends on its location on the silver halide surface. Ag_2 centers on electrically neutral sites trap holes to form Ag_2^+ species. Ag_2 centers at positive kink sites weakly trap electrons and inject holes or are relatively isolated (molecular like).

* To whom correspondence should be addressed: Image Materials & Media, R&D, Eastman Kodak Company, 1999 Lake Avenue, Rochester, NY 14650-1735 Phone: (585) 477-4995. Fax: (585) 477-9674. E-mail: Alfred.Marchetti@kodak.com

It is the intent of this investigation to elucidate the structure and function of some of the sulfide-containing centers created during the sulfur sensitization of AgBr. Specifically, the structure and photophysics of one or more simple sulfur-containing sensitivity centers are sought, that is, centers at which a photographic latent image forms. To that end, photographic behavior has been measured on cubic, octahedral, and tabular (double-twin) microcrystals as a function of the sulfur level. The same samples have been probed by low-temperature photoluminescence (LTPL), optically detected magnetic resonance (ODMR), radio-frequency photoconductivity (rfPC), dielectric loss (DL), ionic thermal current (ITC), and thermally stimulated current (TSC) spectroscopy. Computational techniques have been used to calculate the positions of various sulfide-center HOMOs and LUMOs with respect to the conduction and valence bands of AgBr and thus their potential behavior as electron or hole traps. A short primer on simple photographic and photophysical behavior of silver halides can be found in ref 2.

Previous studies of sulfur sensitization are numerous.[3−26] Many of these studies were not directed toward an understanding of the structure and functioning of sulfur-containing centers. Many studies employ $S_2O_3^{2-}$ as a sulfur source and are confounded by an activation energy for surface adsorption and an activation energy for decomposition that are similar.[8] In the last dozen years, several groups of investigators have applied photographic and various photophysical techniques to sulfur-sensitized silver halide microcrystals in an effort to define the behavior of the sulfur centers.[14,15,18−20,26] Scanned and chopped

10.1021/jp026112p CCC: $25.00
Published on Web 12/11/2002

far-IR light was used to modulate the visible luminescence from band-gap-excited silver halide microcrystals at LHe temperatures.[14,15] This technique is an extension of previous IR absorption and Zeeman spectra that characterized shallow (Coulomb) traps in AgBr.[16,17] From the IR excitation spectra of sulfur-sensitized microcrystals, it was shown that there was an electron-trapping species whose binding energy was ~0.2 eV. The dependence of signal intensity on sulfur level was interpreted as indicating that this species contained two sulfur atoms. These modulation spectra further indicated that there was another electron-trapping species with a binding energy of ≤0.7 eV and a hole-trapping species with a trap depth between 0.5 and 1.0 eV. These researchers proposed two groups of sensitizers: deep electron traps such as S centers (several structures are proposed) and hole traps such as Ag_2 centers. It was conjectured that a substitution sulfur dimer with compensating interstitial silver ions was the primary electron trap.

Diffuse reflectance spectra, microwave photoconductivity at −100 °C, and photographic behavior after redox buffer treatment were used to probe sulfur centers, and these were used as a basis to propose models for the centers.[18,19,26] It was concluded that Ag_2S centers "in the surface" trap holes, $(Ag_2S)_2$ centers in the surface compensated by interstitial silver ions are the sensitizer centers, and $(Ag_2S)_x$ ($x > 2$) clusters are fog centers, that is, centers that cause development without exposure. Na_2S was substituted for $S_2O_3^{2-}$ in some experiments and that should have eliminated most of the heat activation problems. In 1998, two researchers used more sophisticated diffuse reflectance spectroscopy to examine the sub-band-gap absorption observed in AgBr microcrystals that have been treated with high levels of sulfide.[20] They also used 4-hydroxy-6-methyl-1,3,3a,7-tetraazaindene (TAI) to suppress the formation of this long-wavelength feature. They conclude that the reflectance spectra previously obtained were actually composites of contributions from three species. They proposed models of dimers and trimers of Ag_2S with various degrees of charge compensation by interstitial silver ions. In a recent article, researchers "soft landed" $Ag(Ag_2S)_x^+$ ($x = 1$ to 6) clusters on silver halide microcrystals and observed the photographic behavior.[24] The scatter in the data and the checks are not as consistent as one would like, but this work provides clues to sulfur cluster behavior as a function of size. Finally, a just published work details sulfur sensitization studies on AgBr octahedral microcrystals.[25] This work presents spectra obtained by direct absorption that resemble those found in ref 20.

All of this work suggests, as have previous investigations, that sulfur dimers may play a key role in sulfur sensitization. Unfortunately, sensitometric data is very indirect, and many photophysical techniques did not provide microscopic or structural information. The deficiency in all of these investigations is the lack of data that can provide microscopic information about the centers and their function. Thus, the proposed structures lack specificity and testability. It is expected (on the basis of investigations on reduction sensitization) that the position and site of the sensitizer center along with its size will play a key role in its function.[1]

In the next section, we outline the experimental methods used to probe the sulfur centers deposited on the AgBr surface. In this same section, the computational methods used are outlined, and the models for the AgBr surface on or in which the sulfur centers are deposited are discussed. The following section details the predictions from the computations and sets forth the experimental results. The final section discusses these results and makes comparisons with the computational predictions.

TABLE 1: Physical Data on the Three Types of Microcrystals Used in This Investigation

name	description[a]	vol. (μm^3)	surf./vol. (μm^{-1})
OCT	0.50-μm AgBr octahedra	0.059	14.7
CUB	0.40-μm AgBr cube	0.064	15.0
TAB	2.7- × 0.07-μm AgBr tabular	0.40	30

[a] The microcrystals used in this study were monodispersed with variation coefficients of less than 0.08. The OCT and CUB sizes are given as edge lengths, and the TAB size is given as an equivalent circular diameter and thickness even though most of these microcrystals are hexagonal plates.

Experimental Section

A description of the AgBr microcrystals used in this study is given in Table 1.

These AgBr microcrystal dispersions in gelatin were fabricated by a double jet addition of solutions of $AgNO_3$ and NaBr to a stirred reaction vessel containing gelatin at temperatures between 50 and 70 °C.[27] The bromide ion concentration is used to control the morphology. Low bromide ion concentrations (10^{-4} M) favor cubic (001) morphologies whereas higher bromide ion concentrations (10^{-2} M) favor octahedral (111) morphologies. Nucleation at somewhat higher bromide ion concentrations (4×10^{-2} M) causes the formation of parallel twin planes that engender a tabular morphology with (111) surfaces.

Small batches (0.1 M) of the three microcrystal dispersions were treated with various levels of a labile sulfur compound, carboxymethyltrimethyl-2-thiourea (CTT).[28] The levels of CTT used correspond to formal depositions of 0, 1K, 2K, 5K, 10K, 20K, 50K, and 100K sulfur atoms per μm^2. In some experiments, low levels of 4-hydroxy-6-methyl-1,3,3a,7-tetraazaindene (TAI), a material that complexes silver ions, were added before or after the sulfur reaction. The microcrystal dispersions were then processed by heating for either 5 min at 40 °C or ramped at 1.66 °C/min to 65 °C and then held for 20 min and chill set.

Coatings were prepared for sensitometry and radio-frequency (rf) photoconductivity measurements. The microcrystal dispersions were coated on poly(ethylene terephthalate) (Estar base) with a gelatin overlayer. The coating laydowns were 1.61 g Ag/m^2 and 3.23 g gelatin/m^2. Bis[1,1′-[methylenebis(sulfonyl)] (BVSM) (1.8 wt %) was added to the gelatin overcoat (1.61 g gelatin/m^2) to cross link and thereby harden the gelatin. From the same batch of microcrystals, castings were made for DL, ITC, and TSC measurements. The casting format was 38.74 g Ag/m^2, 32.28 g gelatin/m^2, and 10.8 g/m^2 POL-4455, a polyacrylamide latex polymer added to make the casting flexible in vacuum. A small sample of the microcrystal dispersion from each batch finish was used for LTPL and ODMR measurements. The sensitometric (photographic) analysis was a measurement of the reciprocity behavior with visible-light exposures from 10^{-3} to 10 s through a UV cutoff (Kodak Wratten 2B) filter. To obtain reciprocity behavior, film strips are exposed through a stepped neutral density filter (0.3 density steps) with the same number of photons but with different exposure times, in this case, times from 10^{-3} to 10 s in decade increments. The coatings were then processed for 6 min in a Kodak rapid X-ray developer (KRX).

rfPC is a technique that responds to free or very shallowly trapped electrons (or holes under the correct conditions).[29] For free electrons, the response is proportional to the number density and mobility. For trapped electrons, the response is proportional to the number density and polarizability. Thus, this technique can give information about electron lifetimes and the trapping

ability of materials such as sulfur centers added to the surface. The photoelectron response of the microcrystals treated with various sulfur levels was measured at $T = 298$ K using this technique. The samples were exposed with an ~2-μs pulse from a Xenon flash lamp. If the magnitude of the photoelectron response allowed, the exposure was made with a UV filter (280−390-nm band pass) in place; otherwise, the full spectrum available from the lamp was used. The photoelectron response was quantified as the maximum photoconductivity signal (S_{max}) in mV. For some of the microcrystal coatings, a neutral density filter was used to reduce the photoconductivity signal to a point where the resonant circuit was not overdriven.

In AgBr, there are mobile interstitial silver ions. The ionic conductivity due to interstitial silver ion motion in the microcrystals was probed using the standard dielectric loss measurement.[30] The measurements were made on free-standing gel castings of the microcrystals. For a dielectric loss experiment, these castings become the dielectric in a capacitor, and the real and imaginary parts of the dielectric constants are measured as a function of frequency and temperature. From these data, the loss tangent is calculated. Peaks in the dielectric loss as a function of frequency are related to the ionic conductivity of the silver halide microcrystal in the casting. An Arrhenius plot of the microcrystal ionic conductivity−temperature product yields an enthalpy that is the combination of the interstitial silver ion formation and motion enthalpies.

Ionic conductivity was also probed via a qualitative method—ITC.[31] In this method, a casting is again mounted in a capacitor. An electric field (an applied potential of 30 V) is applied, and the sample is cooled to $T = 20$ K. A polarization is thus frozen into the sample by any polar or ionic species in the sample that can move under the force of the field. Once the sample is at 20 K, the field is removed, and the sample is warmed at 7 K/min back to room temperature. As the various species gain thermal energy, they start to move, and the sample depolarizes. This typically gives rise to a characteristic depolarization spectrum as a function of temperature. Empirically, it has been shown that, for silver halide microcrystal samples, in gelatin the temperature of the peaks in these spectra correspond directly to the enthalpies from dielectric loss. A closely related technique—TSC depolarization—allows a qualitative probe of photocarrier trapping states in a microcrystal. In this method, the sample is first cooled to $T = 40$ K, at which time the field is applied (an applied potential of 30 V) and the sample is exposed for 5 min to a 400-nm light source (a 400-nm interference filter on a 500-W xenon lamp). The light and the field are then turned off, and the sample is cooled to $T = 15$ K. As with ITC, the sample is then warmed at 7 K/min, and the depolarization current is monitored. As the trapped photocarrier becomes thermally stimulated, depolarization peaks are observed that qualitatively represent the density of trapping states in the microcrystal.

Low-temperature luminescence spectra were obtained with a small amount of the microcrystal dispersion placed in a sample holder in a metal double Dewar. Most of the measurements were made at 6 K. Luminescence spectra were obtained by exciting the sample with light from a xenon lamp double-monochromator system or with the light from one of several gases. The emission is collected and chopped and then directed into a computer-controlled $^3/_4$-m spectrometer/photomultiplier. The spectra are corrected for the spectrometer/photomultiplier response. Excitation spectra were obtained by monitoring the luminescence intensity at a specified wavelength while scanning the excitation spectrometer. Excitation spectra were corrected for the lamp/spectrometer.[1]

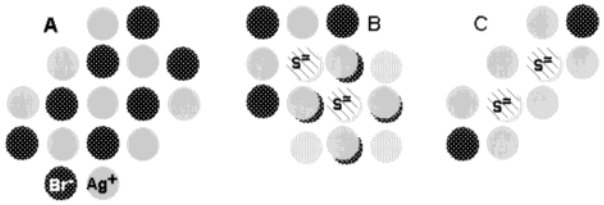

Figure 1. Top views of quantum mechanical models of (A) Ag_9Br_8 representing the (001)AgBr surface. (B) The Ag_7Br_7 double-kink model showing how a Ag_4S_2 molecule builds into the kink. A 3 × 3 array of nine ions is under the Ag_4S_2 moiety. (C) Top layer of the $Ag_8Br_2S_2$ model used for treating the Ag_2 molecule adsorption. Underlying the top layer are two silver ions below the S atoms. Ag^+ ions compensating the sulfurs are not shown.

ODMR measurements were obtained with the sample positioned within a split-coil superconducting magnet that provides fields up to 20 kG (2 T) in a liquid helium Dewar. Typical sample temperatures were 1.7 K. Samples were positioned at the end of a waveguide connected to a klystron, which provides microwave radiation at 36 GHz. The microwave radiation was modulated at audio frequencies (50 to 10 000 Hz). Optical excitation was provided by a helium−cadmium or an argon ion laser. The emission was collected by a lens through appropriate filters and directed onto a photomultiplier (PMT) or into a spectrometer and PMT. The output from the PMT was fed into a lock-in amplifier that was referenced to the microwave modulation frequency. A computer was used to collect and display the data from the lock-in amplifier and to control the magnetic field.[1]

Computations

The structure and energy levels with respect to the conduction and valence bands of AgBr of several species that may be formed during sulfur sensitization have been calculated. The exact species formed on the surface are not conclusively known from experiment, so a number of plausible species were examined. These include the Ag_2S and Ag_4S_2 molecules that may be adsorbed at a flat terrace on the surface or next to a defect such as a kink or ledge. Alternatively, the deposited sulfide ion may become incorporated into a surface, replacing a bromide ion. Such a substitution requires a compensating positively charged species because of the differing sulfide and bromide charges (valance). Charge compensation by a silver ion on the surface or in interstitial positions next to the surface sulfide is considered. Single isolated sulfide ions and pairs of sulfide ions on adjacent bromide sites were considered. All of these species are treated within the framework of a small cluster of silver and bromide ions, described quantum mechanically, that is embedded in an array of several thousand point-ions representing the remainder of the crystal surface region.

A brief description of the models treated is presented below; a more complete discussion has been published.[32] We consider the (001) cubic AgBr surface because its structure is understood.

A (111) surface may be considered to be a collection of (001) surfaces with kinks, ledges, et cetera.[33] The Ag_9Br_8 planar quantum model shown in Figure 1A is employed to treat Ag_2S or Ag_4S_2 molecules adsorbed on a (001) surface. The Ag_2S or planar Ag_4S_2 molecule is placed on top of the quantum model, and its optimum geometry corresponding to the stationary energy point is found. These molecules are also considered to be next to a double-kink defect site, where a new optimum geometry is calculated with the Ag_7Br_7 double-kink model. This model is

shown in Figure 1B and indicates how the adsorbed Ag_4S_2 molecule can start to become incorporated into the crystal lattice. This surface defect site is considered to be representative of sites that may exist on the surface, and we attach no specific importance to this site as compared to several similar sites that may exist. In the case of sulfide ions substituted into the (001) surface, the $Ag_8Br_2S_2$ model shown in Figure 1C is treated. Two silver ions in the second plane are situated under the sulfides. We have studied silver ions on the surface or in interstitial sites next to the sulfide in this model in order to achieve compensation. In addition to the double-sulfide models shown, comparable single-sulfide models were treated. In each model, the quantum mechanical unit is embedded in a hemispherical array of point charges such that the entire unit has zero charge. In addition, the positive point-charges adjacent to the halide anions are replaced by a full silver ion pseudopotential to reduce possible artificial polarization effects, as discussed earlier.[34]

A density functional calculation (B3LYP) is employed to find the total energy and charges of ions of the cluster.[35] We employ a model potential to represent Ag with a double-ζ plus polarization valence basis set,[36] the lanl2dz basis, and the pseudopotential of Hay and Wadt for Br and a full double-ζ basis for S.[37] The total energy of the cluster is taken as a sum of the quantum mechanical part and a relaxation component due to the polarization of the embedding lattice. This part is calculated classically using a shell-model representation of AgBr in which the lattice ions relax in the presence of the fixed ions of the quantum mechanical cluster. This classical calculation is performed with the MIIDAS/CHAOS code, and the quantum mechanical part, with the CADPAC code.[38,39] The total energy of the appropriate charge states is subtracted to determine the ionization potential (IP) or electron affinity (EA). We employ reference levels of 3.6 eV for the conduction band edge and 6.2 eV for the valence band edge, as in previous work, where a more detailed description of the embedding type of calculation is available.[34]

Results

Computations. The Ag_2S and Ag_4S_2 molecules were found to adsorb to the (001) AgBr surface, with S atoms roughly on top of silver ions and silver atoms on top of bromide ions. We calculate IP = 6.7 eV and EA = 3.2 eV for Ag_2S. This species should not trap electrons or holes given these values. For Ag_4S_2, we calculate IP = 5.2 eV and EA = 3.4 eV. In this case, holes can be trapped with a depth of 1.0 eV, but electrons would not be trapped. When these molecules are adsorbed next to a double kink, they start to become part of the crystal lattice. In this case, Ag_2S remains inert, but Ag_4S_2 has IP = 5.9 eV and EA = 4.3 eV. Thus, either electrons or holes can be trapped on the Ag_4S_2 species next to the double kink. The Ag_4S_2 molecule has started to build into the crystal lattice in this species. As the Ag_4S_2 builds further into the double kink, trapping properties change. These data are tabulated in Table 2.

We now turn our attention to sulfide ions substituted for bromide in the (001) surface. Silver ions at interstitial sites next to the sulfide are compensating species. We compute IP = 6.4 eV and EA = 3.0 eV for a single isolated sulfide ion and IP = 5.4 eV and EA = 2.9 eV for two sulfide ions on adjacent bromide sites. The disulfide species could trap a hole with a depth of 0.8 eV, but it cannot trap electrons. The single sulfide species cannot trap electrons or holes. These data are also found in Table 2.

Consider two substitutional sulfide ions that are compensated by silver ions on the (001) AgBr surface. This disulfide species is shown in Figure 2 nearly along the (110) direction. The two adjacent sulfide ions are separated by 4.05 Å, and the silver ions are positioned according to their optimum energy. Table 3 gives the optimized positions and corresponding electron affinity for several charge states of the two compensating silver ions.

TABLE 2: Calculated Transition Energies from the Ground State to the First Singlet (S_1) or the First Triplet (T_1) State and Summary of Trapping Ability for Several Sulfur Centers[a]

species[b]	S_1 (eV)	T_1 (eV)	e^-_{trap}	h^+_{trap}
Ag_2S free (= gas phase)	2.57	2.10	n	n
$Ag_2S(001)$	2.74	2.13	n	n
Ag_2S DK	3.39	2.88	n	n
Ag_4S_2 free	2.33	2.00	n	y
$Ag_4S_2(001)$	2.33	1.86	n	y (1.0 eV)
Ag_4S_2 DK	2.59	2.15	y (0.7 eV)	y (0.3 eV)
Ag_4S_2DK in lattice			y (0.4 eV)	n
S K^+ Ag^+_{int}			y (shallow)	n
S_{sub} bulk Ag^+_{int}	4.70		n	n exciton trap (22)
$2S_{sub}$ bulk $2Ag^+_{int}$			n	y
$S_{sub}(001)Ag^+_{int}$	4.44		n	n
$2S_{sub}(001)2Ag^+_{int}$	3.72		n	y (0.8 eV)
$2S_{sub}(001)2Ag^+_{surf}$	2.34		y (1.3 eV)	n
$2S_{sub}(001)2\perp Ag^+_{surf}$			y (0.6 eV)	n

[a] Calculated trap depths are given in parentheses. [b] DK = double kink site, K^+ = positive kink site, Ag^+_{int} = interstitial silver ion.

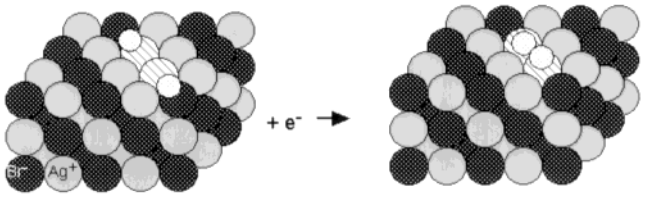

Figure 2. View of adjacent sulfides in the surface showing the positions of the adsorbed silver ions (represented by small dotted circles against a white background) before and after the addition of an electron.

TABLE 3: Calculated Properties of Ag_2 Molecules Adsorbed to Disulfide in the Embedded $Ag_8Br_2S_2$ Model[a]

	Ag−Ag bond along the S−S axis		
molecule	R_1 (Å)[b]	R_2(Å)[b]	EA (eV)
Ag_2^{2+}	6.32	2.45	4.87
Ag_2^+	2.74	2.52	2.88
Ag_2	2.67	2.63	

[a] The Ag−Ag bond perpendicular to the S−S species bond was found to be less stable. [b] R_1 is the Ag−Ag distance, and R_2 is the Ag−S distance.

The two silver ions are well separated at 6.32 Å in the totally compensated state. This state has the ability to trap a photoelectron, as shown by its electron affinity. When an electron is trapped, the silver ions move to within 2.74 Å, forming a bond that is similar to that in Ag_2^+. The possibility of trapping a second electron was also considered, but the calculated electron affinity is too small for this state to be stable. This hypothetical state is calculated to have an even smaller bond length than Ag_2^+. Also considered was a configuration in which the silver ions were placed at a right angle to the axis of the sulfide ions. This species was also calculated to have the ability to trap one electron to form Ag_2^+. It was found to be 0.74 eV less stable than the parallel species, so only the parallel state was optimized for all charge states.

Finally, we have examined a hypothetical kink model of a sensitizing center that contains a sulfide ion and the corresponding compensating interstitial silver ion, shown in Figure 3, to

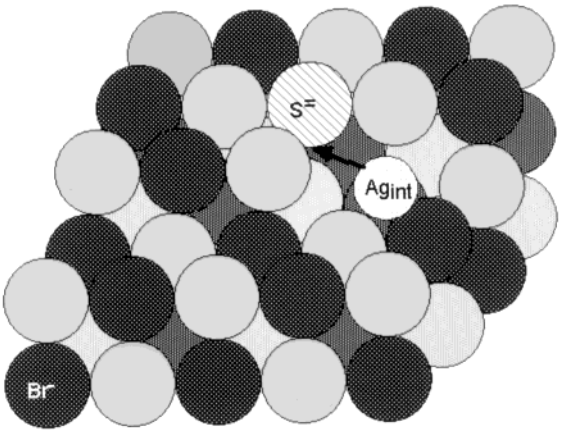

Figure 3. Model of a positive kink with a sulfur substituting for a bromide ion. The compensating silver interstitial is down and behind the sulfur atom.

TABLE 4: Kink Models for Calculated Energy Change (eV) upon Silver Cluster Formation at an Ordinary Positive Kink (+K) and at a Positive Kink with a Sulfur at the Origin Plus a Compensating Ag^{+}_{int} (+SK)

reaction	ΔE (eV) at +SK	ΔE (eV) at +K
(1) $Ag^0 + e^- \rightarrow Ag^-$	−1.4	−1.3
(2) $Ag^- + Ag^+_{int} \rightarrow Ag_2$	−0.32	−0.29
(3) $Ag_2 + e^- \rightarrow Ag_2^-$	−0.16	−0.20
(4) $Ag_2^- + Ag^+_{int} \rightarrow Ag_3$	-0.46	+0.08
(5) $Ag_3 + e^- \rightarrow Ag_3^-$	−0.72	−0.6
(6) $Ag_3^- + Ag^+_{int} \rightarrow Ag_4$	−0.35	−0.63
(7) $Ag_4 + e^- \rightarrow Ag_4^-$	−0.83	−0.37

determine the thermodynamics of latent image growth at such a site. A latent image site, which is a site that catalyzes development, has been shown to be a cluster of four or more silver atoms.[40] The sulfide is substituted for a bromide ion, and the interstitial silver ion is in the lower layer behind the sulfur. A scheme of alternating electron and silver ion addition to the site is considered. We start with a silver atom at the site since the initial formation of the atom is inferred from photoconductivity experiments.[41] The thermodynamics of latent image growth at this site is compared to the hypothetical plus kink model. Consider the sequence shown in Table 4, in which the calculated energy changes are shown on the right side of the equations. A negative value indicates an exothermic reaction. In all cases, the +SK reactions are exothermic. Table 4 shows similar results in terms of overall reaction exothermicity at a positive kink site except for reaction 4, so we can say that the presence of sulfide may improve the energetics of latent image formation. These computations indicate no thermodynamic barrier to latent image formation at the positive kink site containing a sulfide ion. This model is a plausible sensitizing site for a latent image, but we cannot exclude other possible models such as the disulfide at a double kink (Table 2) that may have a series of exothermic reactions leading to a four silver atom cluster. The protruding end of this cluster resembles a sulfur atom at a positive kink.[32]

We studied the properties of the silver dimer at some of the various surface defect sites discussed above because this center is believed to be formed under reduction sensitization. Thus, we wished to learn whether this center would be stable at various sites containing sulfur. The adsorption energy was computed from the difference in energy of the sum of the gas-phase Ag_2 plus the defect-site model and the energy of the optimized Ag_2 at the defect site. Data for several sites are presented in Table 5.

TABLE 5: Adsorption Energy (eV) Calculated for Ag_2 Dimers at Various Sites on the AgBr Surface

site	adsorption energy (eV)
+K	1.5
+K with S, Ag^+_i (Figure 3)	1.4
+K with 2S, $2Ag^+_i$	1.4
DK	1.2
DK with Ag_4S_2 built into crystal	1.8
$2S_{sub}$ with $2Ag^+_i$	0.8
(001) surface	0.4

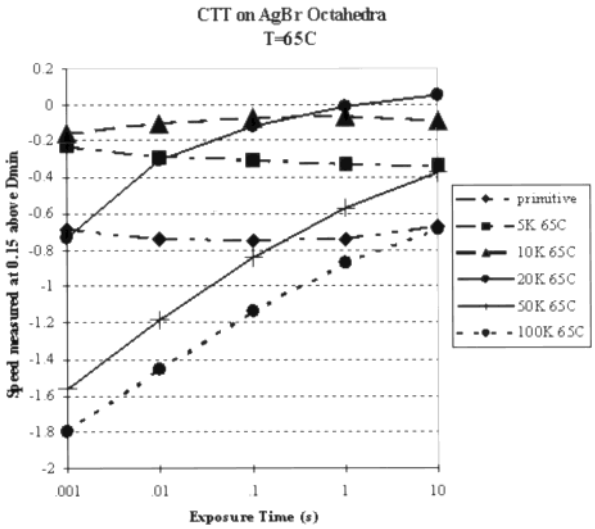

Figure 4. Reciprocity behavior with the photographic speeds measured at a density of 0.15 above the minimum density level of the coated OCT microcrystal dispersion for a processing temperature 65 °C with CTT as the sulfur source. The photographic speeds are relative log values.

These results indicate that surface sites containing S can favorably bind the Ag_2 molecule. Kink-like sites containing S are most favorable. We believe that reasonable sites on the AgBr surface were considered, but since the concentration of these sites is unknown, it is not possible to deduce the overall surface composition.

Photographic. Figure 4 shows the photographic reciprocity data for the sulfur series on AgBr OCT microcrystals. For both the 40 and the 65 °C processing, the optimum photographic speed occurs between 10K and 20K sulfur atoms/μm^2 with the actual optimum much closer to 10K S atoms/μm^2. This is inferred from the fact that for the 20K series the onset of weak high-intensity reciprocity failure (HIRF) is seen.[2] At the higher sulfur levels, the HIRF becomes severe and indicative of oversensitization, with several latent image centers forming on each microcrystal. It is generally understood that some optimum number of sulfur centers per unit area will produce a more or less uniform increase in photographic speed with approximately one latent image site per microcrystal at various exposure times. As the optimum number of sulfur centers is exceeded, the probability that the latent image will initiate at several sites increases, and a given microcrystal will require more photons to become developable. This is most pronounced at short exposures (high intensity), hence the name HIRF. For all of the sulfur levels studied, the minimum optical density (D_{min}) values of the developed coatings were low—less than 6% of the maximum density (D_{max}). D_{min} is a measure of those grains that are made developable by the sensitization process without light exposure. D_{min} is usually expressed as a percentage of D_{max} that will occur upon complete exposure.

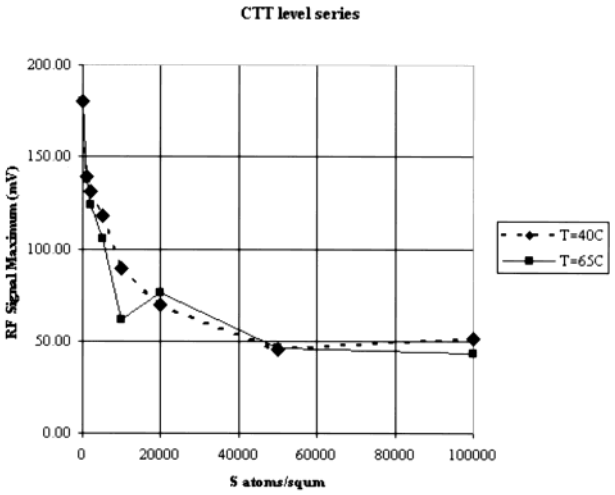

Figure 5. rf photoconductivity response of the AgBr OCT microcrystals for both the 40 and 65 °C sulfur sensitization series. No filters were in place.

The photographic reciprocity data for the sensitization series on the AgBr CUB microcrystals is similar to that for the microcrystals with an octahedral (111) surface. For the sensitizations at 40 °C, the optimum appears to occur at a high sulfur level, close to 50K sulfur atoms/μm^2. This may be because labile sulfur compounds typically react somewhat slower or less efficiently on cubic surfaces.[42] At the lower sulfur levels, all of the sensitizations showed a small amount of low intensity reciprocity failure (LIRF) whereas at the highest sulfur-level studied weak HIRF was encountered. For all of the sulfur levels studied, the D_{min} values were <6% of D_{max}. The data for the 65 °C heat digest exhibited a different response to the sulfur level, with an optimum somewhere between 10K and 20K S atoms/μm^2 but with severe HIRF setting in at 50K S atoms/μm^2. Unlike the octahedral microcrystals, there was some fog growth as the sulfur level was increased, but it was still not severe, with the highest fog level corresponding to about 10% of D_{max}.

The photographic data for the 40 °C sensitization series on the AgBr TAB microcrystals showed no significant reciprocity failure until the highest sulfur level was reached. The optimum sensitization appears to be close to the 20K S atoms/μm^2. The 65 °C sensitizations were all inferior to the 40 °C sensitizations, with the best speed position about a stop (2×) behind the optimum 40 °C position. Unlike the octahedra and the cube, the tabular microcrystals developed significant fog at the higher sulfur levels, especially for the 65 °C sensitizations. The addition of modest levels of TAI (0.1 to 0.3 mM/M of Ag) to the TAB microcrystals before or after sulfur treatment increased the photographic speed by as much as a factor of 2.

RF Photoconductivity. The rfPC data are shown in Figure 5 for the OCT microcrystal S sensitization series. For AgBr microcrystals at room temperature, the longest electron lifetimes are approximately a few hundred nanoseconds.[43] With a time resolution for the rfPC measurements of <10 μs, what is observed is the decrease in the signal maximum as surface traps are added. For sulfur sensitization, the photoelectron response is significantly attenuated by the sensitization and ultimately is reduced by about a factor of 4. The temperature of the sensitization does not appear to affect the efficacy of the electron trapping significantly. At the two highest sulfur levels, the photoelectron response appears to have reached a nonzero plateau. These data suggest that the deposited sulfur centers are

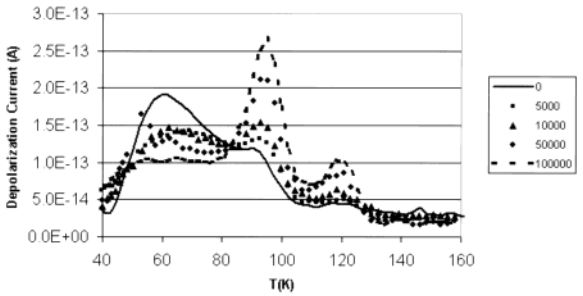

Figure 6. TSC spectrum for an OCT microcrystal showing the effect of the T = 40 °C sulfur sensitization level. (Solid curve is the unsensitized microcrystal dispersion).

significant electron traps and that a majority of the traps are created as a formal level of 10K S atoms/μm^2 is reached.

The rfPC data for the CUB microcrystals also shows an attenuated photoelectron response from sensitization. It is reduced by a factor of 2 at the highest S levels. The temperature of the sensitization does not significantly affect the efficacy of the electron trapping. Even with the full lamp output, the signals are all small. At the two highest sulfur levels, the photoelectron response has again reached a nonzero plateau.

The rfPC data for the TAB microcrystal sensitization series are different from both the CUB and the OCT microcrystals in several ways. The magnitude of the photoelectron signal was substantially larger, and heavy light filtering was in place to position the signal intensity at an appropriate level. The higher levels of sulfur sensitization reduced the photoelectron signal by a factor of 25. This may be due to the larger surface-to-volume ratio of the tabular microcrystals. As with that of the other microcrystals, however, the photoelectron signal was unaffected by the temperature of the sensitization. Finally, rfPC data taken on AgBr/I microcrystals that have a hole response indicate that some of the sulfur centers that are created trap holes. The same results have been observe on AgBr octahedral microcrystals.[44]

Dielectric Loss, Ionic Thermocurrent, and Thermally Stimulated Current. The enthalpies for interstitial silver ion creation/motion were found to be unchanged as function of sulfur sensitization level. The effective ionic conductivities at 298 K were also unchanged with S sensitization. A two-peak dielectric loss spectrum that is unique to (111) surfaces was observed in the octahedral and tabular microcrystals. One peak is believed to be due to ionic motion on or in the microcrystal surface whereas the second peak is due to ionic motion in the subsurface space−charge layer. The cubic microcrystals exhibit only one peak that is thought to be due to ionic motion in the subsurface space−charge layer.[45]

The ITC is a companion to dielectric loss that is far more qualitative but sensitive. There has been established[46] an empirical correlation between the peak temperatures for an ionic depolarization event in ITC and the derived enthalpies from DL. The ITC results as a function of sulfur sensitization for the octahedral, the cube, and the tabular microcrystal dispersion corroborated the dielectric loss enthalpy data.

The TSC spectra as a function of the sulfur sensitization level are more interesting. The TSC spectra for OCT microcrystal as a function of S level are displayed in Figure 6. The unsensitized microcrystal dispersion has a large density of shallow trapping states (broad band at 60 K) with a smaller contribution of deep, ionically neutralized states (the peak at about 92 K). As S centers are added to the surface, the distribution of microcrystal trapping states transitions from mostly shallow trapping to being dominated by the deep, ionically neutralized kind. There was

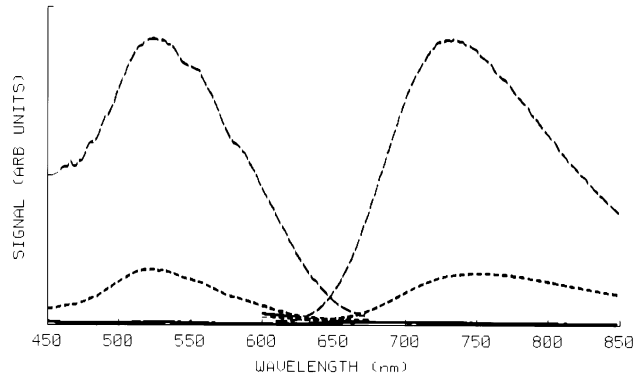

Figure 7. Low-temperature photoluminescence and excitation spectra of the AgBr OCT microcrystal dispersion with various sulfur levels: (—) 100K S atoms/μm^2, (- -) 20K S atoms/μm^2, and (— —) 2K S atoms/μm^2. These samples were heated for 20 min at 65 °C after the addition of CTT. The sample temperature was 6 K, and the excitation wavelength was 515 nm. The 2K S atoms/μm^2 spectra are essentially flat.

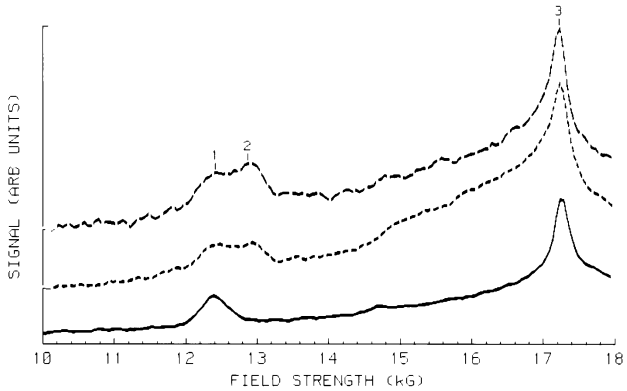

Figure 8. ODMR spectra of AgBr TAB microcrystals untreated (bottom spectrum) and treated with modest levels of sulfur sensitization. The temperature was ~1.8 K, and the modulation was frequency was 170 Hz. The g values as indicated by the tic marks are as follows: (1) $g = 2.08$, (2) $g = 1.99$, and (3) $g = 1.49$. A very weak ICE resonance can be seen at 14.7 kG in some of the spectra.

no substantive difference between the 40 and the 65 °C sensitizations. The CUB and TAB microcrystals gave essentially the same results.

Low-Temperature Photoluminescence. The effects of sulfur sensitization with 40 or 65 °C processing on the luminescence of the octahedral, cubic, and tabular microcrystal dispersions using above band gap 325-, 360-, or 442-nm excitation are to decrease the luminescence peaks at 500 and 590 nm. These luminescence bands are due to the recombination of iodide-bound excitons and donor—acceptor recombination, respectively, and are referred to as the intrinsic luminescence bands. The donors are interstitial silver ions, and substitutional divalent cation impurities and acceptors are thought to be silver ion vacancies.[47] The decrease in intensity is as much as 8- to 10-fold for the highest sulfur levels. The intensity decrease is proportional to formal amounts of sulfur at the lower levels, but the decrease seems to reach a plateau at the higher levels.

The sulfur-related luminescence from OCT microcrystals excited at 515 nm, a photon energy that is below the AgBr band-gap energy, is shown in Figure 7. A long-wavelength emission peaking beyond 700 nm develops as the sulfur is increased to the highest levels. Increasing sulfur levels produce similar increases in the long-wavelength luminescence from TAB and CUB microcrystals. The near-IR sulfur-induced luminescence from CUB microcrystals with a 65 °C digest has the emission-band peak for lower sulfur levels at a slightly longer wavelength (~750 nm), but the emission shifts to ~850 nm for the 100K S atoms/μm^2 level. Modest levels of TAI added before S sensitization prevent the formation of the 525-nm absorption and 725-nm emission. TAI also reduces the intrinsic emission from AgBr microcrystals, indicating that a large fraction of the emission is near-surface radiative recombination.

The emission decayed after pulsed excitation was observed at 670, 720 and 775 nm (700, 750, and 800 nm for the cubes) from several samples. The decay was hyperbolic; that is, log—log plots were characteristic of donor—acceptor recombination.[2] In the 20K and 100K S atoms/μm^2 samples, the peak of the time-resolved emission spectra shifted to lower energies after pulsed excitation by as much as 60 meV (500 cm^{-1}) with delay times up to 900 μs, again characteristic of donor—acceptor recombination. Excitation at 594 nm shifts the emission to longer wavelengths by as much as 50 meV with respect to 515-nm excitation.

Excitation spectra for the OCT microcrystal dispersion are shown in Figure 7. These spectra were obtained by monitoring the emission at ~720 nm. These spectra seem to show a dominant band at ~515 nm and two shoulders at longer wavelengths. The leading edge of the excitation spectra is shifted to longer wavelengths as the monitoring wavelength is moved to lower energies. Similar excitation spectra are seen in the TAB and CUB microcrystals although the excitation spectra from the CUB microcrystals seem to be broadened and the shoulders poorly defined. The excitation spectra were confirmed for the tabular microcrystals by diffuse transmission measurements at 6 K on the TAB microcrystals with 100K S atoms/μm^2. These excitation spectra strongly resemble the spectra inferred from reflectance measurements.[20,25] The new sulfur-associated absorption and emission occur only at high sulfur levels via a reaction that deposits sulfide on or in the first layer of the surface, and the absorption is relatively intense. These facts suggest that the donor—acceptor absorption and emission occur between species on the surface.

LTPL spectra were obtained after samples with 100K S atoms/μm^2 were given a 1-h room-temperature exposure at 633 (1.96 eV), 670 (1.85 eV), or 780 nm (1.59 eV) from a series of diode lasers with relative powers of 1, 3, and 10, respectively. The sulfur-related emission obtained with 515-nm excitation was completely eliminated by the 633- and 670-nm exposure but was untouched by the 780-nm exposure. Exposure at 633 or 670 nm also caused coated microcrystals to develop as if they were exposed to band-gap light. This phenomena is well known for sulfur sensitization.[48] These results indicate that room-temperature excitation into the absorption peaking at ~525 nm causes the promotion of an electron from an acceptor level to a donor level. Some of the electrons promoted to the donor must be thermally detrapped from this level to the conduction band, where they create a latent image. This is suggestive of a thermally shallow donor at room temperature.

Optically Detected Magnetic Resonance. The ODMR spectrum for the untreated TAB microcrystals is displayed in the bottom trace in Figure 8. This spectrum was obtained by monitoring the donor—acceptor recombination emission peaking at ~590 nm. Only two peaks are observed in this spectrum: the donor resonance at 17.2_4 kG with $g = 1.49$ and the acceptor resonance at 12.3_9 kG with $g = 2.08$. These g values are well within the experimental error of the values found for bulk AgBr.[47] Bulk AgBr also often has two additional resonances due to intermediate case excitons (ICE) that are formed for close D—A pairs, and these resonances appear halfway between the donor and acceptor resonances. (These four resonances are often

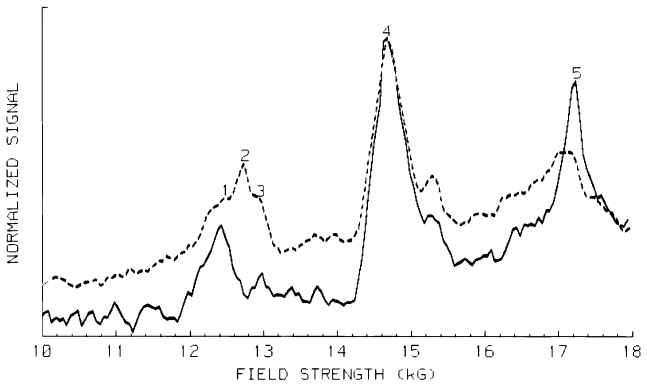

Figure 9. ODMR spectra of AgBr CUB microcrystals untreated (lower spectrum) and treated with 10K S atoms/μm^2. The temperature was 1.8 K, and the modulation frequency was 170 Hz. The donor resonance is evident at 17.20 kG (5), as is the acceptor at 12.43 kG (1) along with an ICE at 14.68 kG (4) in the untreated sample. Two additional resonances are observed in the sulfur-treated sample at 12.73 kG (2) and at 12.93 kG (3). The weak resonance at 15.3 kG ($g = 1.68$) has not been assigned.

referred to as the "intrinsic" ODMR resonances.) The ICE resonances appear very weakly in this spectrum at 14.7 kG. The ODMR spectrum for the AgBr tabular microcrystals treated with 5K S atoms/μm^2 and processed at 65 °C is the middle trace in Figure 8 whereas a sample with 10K S atoms/μm^2 processed at 40 °C is the top spectrum. These spectra clearly display a new resonance at 12.9_4 kG with $g = 1.99$. This resonance is at the identical position within experimental error as the resonance observed in reduction-sensitized microcrystals. That resonance was assigned to an Ag_2^+ species on the basis of the g value.[1,49,50] Similar results were observed for the CUB and OCT microcrystals with both 40 and 65 °C heat treatments. The $g = 1.99$ resonance is observed at a sulfur level that produces no observable sulfur-related emission beyond the band edge. In reduction-sensitized emulsions, the $g = 1.99$ resonance becomes the dominant acceptor resonance at low levels of the reducing agent. At modest reduction sensitizer levels, the intrinsic acceptor resonance is not observed, but in sulfur sensitization, the $g = 1.99$ resonance never becomes dominant. It should be noted that the line width of the $g = 1.99$ resonance is just about broad enough to "cover" the silver hyperfine lines that are normally observed with the Ag^{2+} species.[49]

At higher sulfur levels (20K S atoms/um^2), the intrinsic ODMR resonances becomes weaker, presumably because of decreased emission intensity and the fact that they are more dependent on modulation frequency. For low modulation frequencies (133 Hz), the acceptor resonance at 12.3_9 kG is still observed and is convoluted with the peak at 12.9 kG. Dips in the spectra are sometimes observed at 13.2 and 14.1_5 kG. These "negative" peaks may be artifacts due to spin thermalization.[51,52] Spectra taken at higher modulation frequencies (~1200 Hz) often have only one broad resonance at 15.0_5 kG with $g = 1.71$, but the ODMR signal extends to at least 16.5 kG. The g value of 1.71 is close to the g value for the intermediate-case exciton observed in reduction-sensitized microcrystals, but the shape of this resonance is very different, and it is thought that this resonance(s) is due to other sulfur-related species.

The ODMR spectra of CUB microcrystals with and without sulfur sensitization are shown in Figure 9. The unsensitized material exhibits a donor resonance at 17.20 kG ($g = 1.49$), an acceptor resonance at 12.43 kG ($g = 2.07$), and an ICE resonance at 14.68 kG ($g = 1.76$). In the sample treated with 10K S atoms/μm^2 additional resonances are observed at 12.8_8 kG ($g = 1.99$) and at 12.70 kG ($g = 2.02$). It should be noted that the $g = 1.99$ resonance (the Ag_2^+ species) is not observed on reduction-sensitized cubic surfaces.[1] This suggests that this Ag_2^+ species associated with a sulfur center differs from the species produced in R sensitization. In the reduction sensitization case, Ag_2 is a hole trap (acceptor) that forms an ICE at $g = 1.73$ with the shallowly trapped electron ($g = 1.49$ donor) whereas in the sulfur-related case the silver dimers appear to be electron traps (Ag_2^{2+}) and no ICE at $g = 1.73$ is observed. A resonance is often observed at $g = 2.02$ in the sulfur-sensitized cubic and other microcrystals, which could be an ICE formed between the electron trapped ($g = 1.99$) at the sulfur center and the intrinsic hole trap at that has a g value of 2.07. There are some problems with this straightforward interpretation that will be discussed below, and it is possible that the resonance that is observed at $g = 2.02$ could be due to another sulfur-containing center that can be created by exposure to above band-gap light and whose EPR spectrum occurs in this region.[53]

The ODMR spectra observed when monitoring the 720-nm emission are diffuse and weak. The resonance positions depend somewhat on the monitoring wavelength, and the strongest signals occur with monitoring wavelengths between 750 and 775 nm. There are three or possibly four ODMR resonances. The highest field resonance is at 15.6 ± 0.4 kG ($g = 1.6$), the next, probably two, resonances are in the region of 11.2 ± 0.8 kG ($g = 2.2$), and then there is what is most probably a half-field line at 5.7 ± 0.4 kG. The most reasonable interpretation of these spectra is that the high-field line is due to a donor and that there is an acceptor resonance near 10 kG, which is merged with the strongest signal at ~12 kG that is due to an intermediate-case exciton. All of these species are thought to be surface centers containing sulfide. This interpretation is supported by the observation of a half-field line that will occur only with an ICE.

Discussion

Experimental Data. The photographic data indicates that efficient sulfur sensitization occurs on (111) surfaces with very little heat input. With the exception of the AgBr cubic microcrystals processed at 40 °C, efficient sensitization occurred at relatively low sulfur levels. The optimum sulfur level was about 10K S atoms/μm^2 in most cases. These data indicate that a relatively low level of sulfur applied to the surface of AgBr microcrystals creates "efficient" electron traps that promoted the formation of a latent image, which in turn, increases the photographic speed by 5×. Assuming an optimum sulfur level of 10K S atoms/μm^2, let us examine the other photophysical responses at this level. For reference, a sulfur level of 10K monomeric S atoms/μm^2 provides an average separation of sulfur atoms of 100 Å or 10 nm. This corresponds to about 27 unit cells. If all of the sulfur atoms were paired, then the average distances would be larger by $\sqrt{2}$.

The rf PC data indicates a high level of electron trapping at sulfur levels (10K S atoms/μm^2) that produce about the optimum photographic speed increase. This is interpreted as an indication that many of the sulfur centers formed are electron-trapping. This was to be expected, as sulfur sensitization enhances the ability of silver halide microcrystals dispersions to "process" photoelectrons.[2] The rfPC data varies among the microcrystal morphologies; this may be due to variations in the surface-to-volume ratio, to edge structure (regions that are not well defined as (100) or (111) surfaces), to the number of surface sites, and to differences in microcrystal structure (twin planes vs 3D). Nonetheless, it seems certain that even at modest sulfur levels

there are a significant number of electron traps formed. rfPC data also indicates that some of the sulfur-containing centers are hole traps.[44]

The ionic conductivity data from DL and ITC measurements are unchanged by sulfur sensitization. That is, the enthalpies for interstitial silver ion creation/motion and effective conductivities were determined to be unchanged as sulfur was added to the surface of the microcrystals. This indicates that the space−charge region is not noticeably affected. This is in contrast to treatment with silver-complexing agents such as TAI that totally change the ionic behavior. These data suggests that the S centers that are created are neutral or fully compensated; that is, they are $(Ag_2S)_x$ or $S_x(sub)xAg_{int}$ centers.

The TSC spectra, however, access the detrapping behavior of the available centers. These spectra indicate that the shallow intrinsic centers that manifest themselves as a peak between 50 and 60 K are becoming less important as the sulfur level is increased. The concentration of the deeper states that are ionically neutralized (peaks at ∼94 and 120 K with (111) surfaces and a peak at 135 K with (100) surfaces) becomes larger as sulfur is added to the surface. This data confirms the interpretation of the rfPC data: deeper electron-trapping states are formed with sulfur sensitization. It is expected that holes created in the light-polarization step of the TSC experiment would be detrapped only at relatively high temperatures (>140 K).

The LTPL spectra show that the intensity of the intrinsic emission bands due to recombination at impurity iodides and donor−acceptor recombination is decreasing as the surface sulfur level is increased. This is indicative of the formation of centers that are competing for photocarriers that would normally recombine through exciton formation or donor−acceptor recombination. One competing decay channel is the new long-wavelength donor−acceptor emission. This emission peaks at ∼725 nm and is observed only with sulfur levels >10K S atoms/μm^2. Excitation spectra peaking at ∼525 nm are obtained by monitoring this emission. The high level of surface sulfide associated with the 725-nm emission indicates that the surface donors and acceptors are probably aggregates of sulfur such as dimers. The fact that excitation into the long-wavelength absorption induced by sulfur sensitization causes latent-image formation indicates that it is the sulfur-related acceptor that is deep. The D−A transition energy for the sulfur-related species may be estimated from the emission and excitation spectra. The donor−acceptor energy (E_{DA}) is given by

$$E_{DA} = E_g - [E_D + E_A] + e^2/\epsilon r$$

where E_g is the band-gap energy, E_D and E_A are the donor and acceptor binding energies, respectively, and $e^2/\epsilon r$ is the normal DA Coulomb interaction where ϵ is the effective dielectric constant, e is the charge on an electron, and r is the separation.[2,54]

The DA transition energy is estimated to be at the point where the normalized excitation and emission cross. This occurs at about 670 nm (1.85 eV) for long delay times and long monitoring wavelengths, which should favor distant pair recombination (so that $e^2/\epsilon r \approx 0$). With $E_g = 2.706$ eV, the sum $[E_D + E_A]$ is equal to ∼0.85 eV. Sulfur-related electron trap depths have been estimated to be ∼0.2 to 0.3 eV, indicating that E_A is ∼0.65 eV.[14,15,48] Previous work has proposed that several "molecular" species are responsible for the 525-nm absorption and the 725-nm emission.[20] This appears now not to be true, and it is probable that the peak and shoulders observed in the excitation and reflectance spectra are more likely broadened transitions from excited levels of the deep acceptor. All of the data strongly supports the fact that the long-wavelength absorption and emission created by sulfur sensitization result from donor−acceptor recombination. This is further supported by weak, broad ODMR signals that were detected when monitoring this emission.

The ODMR data monitoring the intrinsic donor−acceptor emission clearly shows the presence of an Ag_2^+ species even on a (001) surface with low levels of sulfur. The presence of this species, never detected on a (001) surface with R sensitization,[1] and the data indicating that most sulfur centers are electron traps suggest that the trapping species might at first be thought to be something like two neighboring substitutional sulfides with a pair of compensating silver ions. The Ag_2^+ species could be formed when this sulfur-containing complex traps an electron. This electron-trapping center can then form an ICE with the intrinsic hole-trapping center (acceptor). This preliminary interpretation will be examined further below. The ODMR spectra taken on samples with higher sulfur levels suggest a more complex system in which other sulfur aggregates are formed or in which there is inhomogeneous broadening of the ODMR spectra.

Taken together, the experimental data points to the fact that several different electron-trapping species are formed upon sulfur sensitization. These traps are deep compared to the intrinsic traps (>30 meV). Data and simple electrostatics seem to indicate that sulfur-containing centers must be neutral (e.g., Ag_2S) or if they are substitutional for Br^- ions they must be compensated by silver ions. The data also indicates that some sulfur centers trap holes.

Computational. The computations have suggested that some of the simple sulfide centers are involved in photophysical activity and sulfur-assisted latent-image formation in AgBr. There is not a full description of these sulfur-containing centers, as centers with only one or two sulfides were treated. It has been conjectured that centers with more than two or three sulfides are fog centers.[18,19,24] However, it is likely that several different sulfur species may be present on the surface that has been sensitized. Several experimental techniques indicate that sulfur-treated AgBr surfaces can trap holes. Our calculations indicate that Ag_4S_2 on flat terraces or next to a double kink could perform this function. Another possible candidate for this function is two adjacent sulfide ions in the (001) surface compensated by interstitial silver ions. The trap depths calculated for these three cases are 1.0, 0.3, and 0.8 eV, respectively. These values carry some uncertainty associated with the calculation and our lack of a complete understanding of the grain's surface structure and composition. Nevertheless, these values indicate that hole trapping is possible, and this is consistent with experiment. We also note that the single sulfide species are calculated to be inactive in this function (see Table 2).

The predominant role of sulfide centers in sensitization is thought to involve electron trapping. In this regard, Ag_4S_2 next to the double kink is calculated to have an electron trap depth of 0.7 eV. Given the range of possible error in our calculations, this value is consistent with experimental values reported in the range of 0.2 to 0.4 eV, but it is also possible that this is consistent with the deeper trap mentioned in ref 14. As shown in Figure 1B, this situation corresponds to the start of building the Ag_4S_2 molecule into the crystal lattice and leaving a free end of the molecule that is very much like a positive kink in appearance. Indeed, calculations have shown that a positive kink containing sulfur substituted for bromides has properties that enable it to grow a latent image by alternate electron and silver

ion capture in AgBr.[32,41] Thus, the incorporation of molecules such as Ag_4S_2 into the surface at a double kink or ledge seems to be a likely means of forming such sites. These sites are probably in the minority on (001) surfaces given the far greater percentage of surface ions present at flat terraces. Computations predict that a sulfide substituted for a halide ion at a +K can be involved in an energetic ladder that improves the possibility of latent-image formation when compared to the same reaction at a positive kink. It should be remembered that both of the reaction schemes outlined in Table 4 start with a silver "atom" at the kink. This species has not been observed on a AgX surface but has been observed in the bulk at low temperatures.[16]

Sulfide ions in the (001) surface disubstituted for bromide ions are predicted to be an electron trap when they are compensated by surface silver ions but are predicted not to trap an electron when compensated by interstitial silver ions. Calculations indicate that one electron may be captured at the surface silver ions to form Ag_2^+. The electron in this center has a trap depth of 1.3 eV, but calculations show that this center cannot capture a second electron to convert to Ag_2. This could be the species that was observed in the ODMR spectra, but other sites can also bind Ag_2 dimers. It should be pointed out that this finding of a particular stability for Ag_2^+ at the disulfide is quite similar to earlier calculated results at various defect sites on the AgBr surface.[34]

There is an energetic problem with the $2S_{sub}(001)2Ag^+_{surf}$ species being a donor (electron trap) that participates in DA recombination. The calculated trap depth was 1.3 eV, and the potential energy curves for the ground state and the trapped electron state have to have minima at very different silver−silver distances. This information would suggest that the DA emission from this donor and the normal acceptor whose trap depth is approximately 0.3 eV or larger would be in the IR region of the spectrum $\{E_{DA} = E_g - (E_D + E_A) + e^2/\epsilon r = 2.706 - (>0.3 + 1.3) + C \approx 1.1$ eV (>1000 nm)$\}$.[55] A sulfur-containing center that has an associated silver dimer would be a species that should trap a hole to give Ag_2^+, which is the species that is observed in the ODMR. This center could have been created in the actual chemical reaction of labile sulfur compounds on the surface. Another way to create this center is to start with the $2S_{sub}(001)2Ag^+_{surf}$ species and add successive electrons and interstitial silver ions so that a $2S_{sub}(001)2Ag^+_{int}$-Ag_2 species is created. This might occur when the species is irradiated with light at low temperatures. The reaction is outlined as follows:

$$2S_{sub}(001)2Ag^+_{surf} + e^- \rightarrow 2S_{sub}(001)Ag_2{}^+_{surf}$$

$$2S_{sub}(001)Ag_2{}^+_{surf} + Ag^+_{int} \rightarrow 2S_{sub}(001)Ag_2{}^+_{surf}\,Ag^+_{int}$$

$$2S_{sub}(001)Ag_2{}^+_{surf}Ag^+_{int} + e^- \rightarrow 2S_{sub}(001)Ag_{2surf}Ag^+_{int}$$

$$2S_{sub}(001)Ag_{2surf}Ag^+_{int} + Ag^+_{int} \rightarrow 2S_{sub}(001)Ag_{2surf}2Ag^+_{int}$$

The Ag_2 species associated with the sulfur dimer in the surface should appear very similar to the Ag_2 species formed with reduction sensitization, which would explain most of the ODMR behavior. At this point, this is speculation because the spectroscopic signature appears to be that of Ag_2^+. Computations have shown that the $2S_{sub}(001)Ag_{2surf}2Ag^+_{int}$ species is stable; that is, the silver dimer has a positive binding energy to the compensated sulfur dimer.

The computed transition energies for a number of the sulfur species are also listed in Table 2. The treatment of S sensitization is very computationally demanding, which is one of the reasons that larger sulfur-containing clusters were not attempted. In addition, the microcrystal grain surface structure is complicated. Clearly, these facts limit what can be done computationally and remind us to use caution in comparing computational data to experiment. However, the real value of these results comes through comparison and interaction with experimental studies.

Finally, it is interesting to contrast the behavior outlined above for sulfur centers on the surface and the behavior of sulfur centers substituted into the crystalline lattice. Substitutional single sulfides are compensated by interstitial silver ions, and they trap excitons at low temperatures.[17,22,57] Sulfides in the lattice also react with divalent cation impurities to form a substitutional molecule that also appears to trap excitons.[22]

Conclusions

Combining the experimental data and computational results produces a picture of photophysical processes that can occur when sulfide is deposited on a AgBr surface. The photographic data points to an optimum formal level of sulfur on a AgBr surface of about 10K S atoms/μm^2. The various sulfur-containing centers that are deposited on a AgBr surface trap both electrons and holes as well as excitons.[22] The trap depths seem to range from 0.2 to <1.0 eV. The luminescence and ODMR data clearly indicates that the sulfur-related long-wavelength absorption (~525 nm) and emission (~725 nm) are due to donor−acceptor processes. This luminescence is most likely due to surface sulfur-containing donors and acceptors that trap both electrons and holes and then undergo subsequent tunneling recombination. At least one of the sulfur-containing centers either has or allows the creation of a Ag_2^+ center upon light exposure.

The computational data indicates that many of the simple sulfur-containing species trap neither electrons nor holes. This may offer a partial explanation of the need for a rather large number of sulfur atoms to be deposited on a AgBr surface to obtain optimum photographic efficiency. The computational data also provides several reaction schemes that can lead to latent-image formation, and it provides an energetic reason for the improvement in the process with the addition of certain sulfur centers. The computational data further suggests several mechanisms for the creation of a species that is observed in the ODMR spectra as Ag_2^+. The overall picture of sulfur sensitization, which is one of the backbone process in the photographic industry, that emerges is one that is quite complex, with a number of sulfur-containing centers playing a role.

When all of these data are put together, remembering that there are uncertainties in both the calculated and measured trap depths and that the computations encompassed only mono- and disulfur species, the following species can be assigned specific functions. A $Ag_4S_2(001)$ species could be an acceptor participating in the 725-nm DA recombination, but it seems likely that this species would become associated with a kink, particularly on a (111) surface that is thought to be made up of small stepped (001) pyramids.[33] So a significant participation of this species is discounted at this time. Ag_4S_2 DK could be the deeper electron trap observed in ref 14, or it could be a surface exciton trap and/or participate in the surface DA recombination (725-nm emission). Ag_4S_2 DK in the lattice is a candidate for the shallow electron trap mentioned in ref 14 and the donor observed in the

725-nm emission. It is also a likely candidate as a site for latent-image formation although the energetics have not been calculated. S at K^+ is a presumed site for latent-image formation (see Table 4). It is also a likely donor in the 725-nm emission and the shallow electron trap in ref 14. The $2S_{sub}(001)2Ag^+_{int}$ species is a likely candidate for an acceptor participating in the 725-nm emission. An associated interstitial could be removed or blocked by the addition of TAI, thus preventing this center from participating in DA recombination. The $2S_{sub}(001)2Ag^+_{surf}$ species is a candidate for the formation of the Ag_2^+ species that is observed in the ODMR spectra from the "intrinsic" emission at 590 nm, but so are four other sites listed in Table 5. Since the Ag_2^+ species is observed in the ODMR from the intrinsic DA emission at very low sulfur levels ($\leq$5K S atom/μm^2), it seems likely that this species is associated with a monomeric sulfur species or an Ag_4S_2 species formed on sulfur addition.

Finally, it has been shown that a combination of sulfur and gold sensitization can produce a quantum yield for latent-image formation that approaches the theoretical limit, taking into account statistical electron−hole recombination (5 to 6 photons absorbed per microcrystal).[56] This and other treatments that approach the theoretical limit of photographic efficiency must eliminate or make inaccessible all "deep" (>0.6 eV) electron-trapping species. The follows from the fact that the theoretical efficiency necessitates only one latent-image site per microcrystal and that to concentrate all of the available electrons at that site all of the created electrons must visit all of the microcrystals and thus cannot be *deeply* trapped.

Acknowledgment. We are indebted to Charles Boda, Joseph Hodes, Jeri Mount, and Laurel Doty for technical assistance. We acknowledge many helpful discussions with Raymond Eachus and Ralph Young.

References and Notes

(1) Marchetti, A. P.; Muenter, A. A.; Baetzold, R. C.; McCleary, R. T. *J. Phys. Chem. B* **1998**, *102*, 5287.

(2) Marchetti, A. P.; Eachus, R. S. The Photochemistry and Photophysics of the Silver Halides. In *Advances in Photochemistry*; Volman, D., Hammond, G., Neckers, D., Eds.; Wiley & Sons: New York, 1992; Vol. 17, pp 145−216.

(3) Sheppard, S. E. *Photogr. J.* **1925**, *65*, 380.

(4) Bassett, R. A.; Dickinson, H. O. *J. Photogr. Sci.* **1963**, *11*, 239.

(5) Moisar, E. *Photogr. Korresp.* **1970**, *106*, 149, and references therein.

(6) Fatuzzo, E.; Coppo, S. *J. Photogr. Sci.* **1972**, *20*, 43.

(7) Birch, D. C.; Farnell, G. C.; Flint, R. B. *J. Photogr. Sci.* **1975**, *23*, 249.

(8) Cash, D. J. *J. Photogr. Sci.* **1981**, *29*, 133, and references therein.

(9) Spencer, H. E.; Atwell, R. E.; Levy, M. *J. Photogr. Sci.* **1983**, *31*,-158.

(10) Marchetti, A. P.; Collier, S. S.; Crews, N. P. *Photogr. Sci. Eng.* **1984**, *28*, 146.

(11) Harbison, J. M. Unpublished results.

(12) Keevert, J. E.; Gokhale, V. V. *J. Imaging Sci.* **1987**, *31*, 243.

(13) Belous, V. M.; Akhmerov, A. Y.; Zhukov, S. A.; Orlovskaya, N. A.; Sviridova, O. I. In *Proceedings of IS&T*, 47th Annual Conference; Rochester, NY, 1994; p 213.

(14) Kanzaki, H.; Tadakuma, Y. *J. Phys. Chem. Solids* **1994**, *55*, 631.

(15) Kanzaki, H.; Tadakuma, Y. *J. Phys. Chem. Solids* **1997**, *58*, 221.

(16) Brandt, R. C.; Brown, F. C. *Phys. Rev.* **1969**, *181*, 1341. Brandt, R. C.; Larson, D. M.; Croohor, P. P.; Wright, G. B. *Phys. Rev. Lett.* **1969**, *23*, 240.

(17) Sakuragi, S.; Kanzaki, H. *Phys. Rev. Lett.* **1977**, *38*, 1302.

(18) Tani, T. *J. Imaging Sci. Technol.* **1995**, *39*, 386.

(19) Tani, T. *J. Imaging Sci. Technol.* **1995**, *42*, 135.

(20) Van Doorselaer, M. K.; Charlier, E. Papers from the International Congress for Imaging Science, Antwerp, Belgium, 1998. Charlier, E.; Van Doorselaer, M. K.; Gijbels, R.; De Keyzer, R.; Geuens, I. *J. Imaging Sci. Technol.* **2000**, *44*, 235.

(21) Belous, V. M. *J. Imaging Sci. Technol.* **1999**, *43*, 1.

(22) Burberry, M. S.; Marchetti, A. P.; Spoonhower, J. P.; McDugle, W. G.; Nuttall, R. H. D.; Tinti, D. S. *Phys. Rev. B* **1991**, *44*, 9817, and references therein.

(23) Deaton, J. Papers from the International Congress for Imaging Science, Antwerp, Belgium, 1998.

(24) Zhao, X.; Ciu, W.; Peng, B.; Liu, P.; Gao, Z.; Zhu, Q.; Kong, F. *Int. Symp. Silver Halide Technol.* **2000**, 227.

(25) Hailstone, R. K.; Zhao, T.; DiFrancesco, A. G.; Tyne, M. *J. Imaging Sci. Technol.* **2001**, *45*, 76.

(26) Tani, T. *Photographic Sensitivity*; Oxford University Press: Oxford, U.K., 1995.

(27) Berry, C. R. In *The Theory of the Photographic Process*; James, T. H., Ed.; Macmillan Publishing: New York, 1977; Chapter 3. Berry, C. R. U.S. Patent 5,147,771, Sept 15, 1992. Berry, C. R. U.S. Patent 5,210,-013, May 11, 1993.

(28) Herz, A.; Burgmaier, G. U.S. Patent 4,810,626, 1988.

(29) Kellogg, L. M.; Muenter, J.; Hodes, J. M. In *The International East−West Symposium II on the Factors Influencing Photographic Sensitivity*; Society for Imaging Science and Technology: 1988; p c-11. Kellogg, L. M. Hodes, J. M. U.S. Patent 4,788,131, 1988.

(30) Hoyen, H. A. *J. Appl. Phys.* **1976**, *47*, 3784.

(31) Vaala, A. R.; Hodes, J. M. *Photogr. Sci. Eng.* **1981**, *25*, 240.

(32) (a) Baetzold, R. C. *J. Imaging Sci. Technol.* **2001**, *45*, 247. (b) Baetzold, R. C. *J. Imaging Sci. Technol.* **1999**, *43*, 30.

(33) Baetzold, R. C.; Hansen, J. C. Unpublished work. See also Knoppik, D.; Losch, A. *J. Cryst. Growth*, **1976**, *34*, 332. Van Der Voort, E.; Hartman, P. *J. Cryst. Growth* **1990**, *104*, 450.

(34) (a) Baetzold, R. C. *J. Phys. Chem. B* **1997**, *101*, 8180. (b) Baetzold, R. C. *J. Phys. Chem. B* **2001**, *105*, 3577.

(35) (a) Becke, A. D. *Phys. Rev. A* **1988**, *33*, 3098. (b) Lee, C.; Yang, W.; Parr, R. G. *Phys. Rev. B* **1988**, *37*, 785. (c) Johnson, B. G.; Gill, P. M.; Pople, J. A. *J. Chem. Phys.* **1993**, *98*, 5612.

(36) Sakai, Y.; Miyoshi, E.; Klobukwski, M.; Huzinaga, S. *J. Comput. Chem.* **1987**, *8*, 256.

(37) Hay, P. J.; Wadt, W. R. *J. Chem. Phys.* **1985**, *82*, 299.

(38) Tasker, P. W. *Philos. Mag.* **1979**, *39*, 119.

(39) Amos, R. D.; Alberts, I. L.; Andrews, J. S.; Colwell, S. M.; Handy, N. C.; Jayatilaka, D.; Knowles, P. J.; Kobayashi, R.; Laidig, K. E.; Laming, G.; Lee, A. M.; Maslen, P. E.; Murray, C. W.; Rice, J. E.; Simandiras, E. D.; Stone, A. J.; Su, M.-D.; Tozer, D. J. *CADPAC*: The Cambridge Analytical Derivatives Package Issue 6; University of Cambridge: Cambridge, U.K., 1995.

(40) Leisner, A. T.; Rosche, Ch.; Wolf, S.; Granzer, F.; Woste, L. *Surf. Rev. Lett.* **1996**, *3*, 1105.

(41) Spoonhower, J. P.; Deri, R. J. *J. Appl. Phys.* **1985**, *57*, 1968.

(42) Marchetti, A. P.; Collier, S. S.; Crews, N. P. *Photogr. Sci. Eng.* **1984**, *28*, 146.

(43) Deri, R. J.; Spoonhower, J. P. *J. Appl. Phys.* **1985**, *57*, 2806.

(44) Kellogg, L. M. Private communication.

(45) Ohzeki, K.; Urabe, S.; Tani, T. *J. Imaging Sci. Technol.* **1990**, *34*, 136.

(46) Kellogg, L. M. Private communication.

(47) Marchetti, A. P.; Burberry, M. S.; Spoonhower, J. P. *Phys. Rev. B* **1991**, *43*, 2378.

(48) Hamilton, J. F.; Harbison, J. M.; Jeanmaire, D. L. *J. Imaging Sci. Technol.* **1988**, *32*, 17.

(49) Baranov, P. G.; Romanov, N. G.; Khramtsov, V. A.; Vikhnin, V. S. *J. Phys.: Condens. Matter* **2001**, *13*, 2651.

(50) Shields, L.; Symons, M. R. C. *Mol. Phys.* **1966**, *11*, 57. Eachus, R. S.; Symons, M. R. C. *J. Chem. Soc. A* **1970**, 1329.

(51) Davies, J. J.; Nicholls, J. E. *J. Phys. C: Solid State Phys.* **1982**, *15*, 5321.

(52) Cox, R. T.; Davies, J. J. *Phys. Rev. B* **1986**, *34*, 8591.

(53) Eachus, R. S. Private communication.

(54) Thomas, D. G.; Hopfield, J. J.; Augustyniak, W. M. *Phys. Rev. A* **1965**, *140*, 202.

(55) Spoonhower, J. P.; Marchetti, A. P. *J. Phys. Chem. Solids* **1990**, *51*, 793.

(56) Hailstone, R. K.; Liebert, N. B.; Levy, M.; McCleary, R. T.; Girolmo, S. R.; Jeanmaire, D. L.; Boda, C. R. *J. Imaging Sci. Technol.* **1988**, *32*, 113.

(57) Silwczuk, U.; von der Osten, W. *J. Imaging Sci. Technol.* **1988**, *32*, 106.